*Computers and Concrete, Vol. 7, No. 5 (2010) 469-482*
DOI: http://dx.doi.org/10.12989/cac.2010.7.5.469


# Numerical and statistical analysis of permeability of concrete as a random heterogeneous composite

Chunsheng Zhou and Kefei Li*

*Key Laboratory of Structural Engineering and Vibration of China Education Ministry, Civil Engineering Department, Tsinghua University, 100084 Beijing, P.R. China*

*(Received October 24, 2009, Accepted April 2, 2010)*

**Abstract.** This paper investigates the concrete permeability through a numerical and statistical approach. Concrete is considered as a random heterogeneous composite of three phases: aggregates, interfacial transition zones (ITZ) and matrix. The paper begins with some classical bound and estimate theories applied to concrete permeability and the influence of ITZ on these bound and estimate values is discussed. Numerical samples for permeability analysis are established through random aggregate structure (RAS) scheme, each numerical sample containing randomly distributed aggregates coated with ITZ and dispersed in a homogeneous matrix. The volumetric fraction of aggregates is fixed and the size distribution of aggregates observes Fuller's curve. Then finite element method is used to solve the steady permeation problem on 2D numerical samples and the overall permeability is deduced from flux-pressure relation. The impact of ITZ on overall permeability is analyzed in terms of ITZ width and contrast ratio between ITZ and matrix permeabilities. Hereafter, 3680 samples are generated for 23 sample sizes and 4 contrast ratios, and statistical analysis is performed on the permeability dispersion in terms of sample size and ITZ characteristics. By sample theory, the size of representative volume element (RVE) for permeability is then quantified considering sample realization number and expected error. Concluding remarks are provided for the impact of ITZ on concrete permeability and its statistical characteristics.

**Keywords:** concrete; permeability; interfacial transition zone (ITZ); random aggregate structure (RAS); finite element method (FEM); representative volume element (RVE).

## 1. Introduction

Permeability is the most important durability parameter for concrete materials (Reinhardt 1997, AFGC 2007). Modern concretes have rather low water to cement(binder) ratio, high density and low permeability. The experimental setup for permeability measurement of concrete materials is not trivial (El-Dieb and Hooton 1995, Kollek 1989), and direct permeability measurement, gas or water, for dense concretes can encounter practical difficulties. Accordingly, accurate prediction of concrete permeability can be very helpful for concrete material design.

Concrete is a heterogeneous composite with about 70% volume occupied by fine and coarse aggregates randomly distributed in space. Multi-scaled modeling is well accepted for concrete composite (Maekawa *et al.* 2009). At centimeter scale, concrete can be regarded as a three-phase composite: coarse aggregates, mortar and interfacial transition zones between them; at millimeter or smaller scale, mortar itself can be considered as a three-phase composite: fine aggregate, cement

* Corresponding author, Associate Professor, E-mail: likefei@tsinghua.edu.cn

paste and the interfacial transition zone between them. Normally the permeability of aggregates is several magnitudes lower than mortar matrix or cement paste (Powers 1958). The interfacial transition zones around aggregates are formed by "wall effect" of cement grain packing against aggregate surface, thus local higher water content renders hardened paste more porous and rich in $Ca(OH)_2$ crystals (Scrivener 1988, Ollivier *et al.* 1995). The substantial impact of ITZ on concrete mechanical behaviors has been extensively investigated and confirmed (van Mier 1997, Nemati *et al.* 1998). The ITZ has also been subjected to extensive research on its geometrical characteristics (Bentz and Garboczi 1991, Scrivener 2004, Hu and Stroeven 2004, Nemati and Gardoni 2005), its local transport properties (Snyder *et al.* 1992, Bourdette *et al.* 1995, Yang and Su 2002) and its influence on the material physical properties (Garboczi *et al.* 1995, Schwartz *et al.* 1995, Delagrave *et al.* 1997). On the basis of the above results, this paper proceeds to quantify the material overall permeability in a statistical context. Quantitative prediction of permeability of a random heterogeneous composite includes two fundamental aspects: the material structure-permeability relationship and the variance of predicted permeability. These two aspects are treated successively in this paper: some classical bound and estimate theories are firstly reviewed and applied to concrete in Section 2; in Section 3 numerical samples are generated by random aggregate structure scheme and finite element method is used to solve the 2D permeation process; then numerical sampling is performed in Section 4, the statistical characteristics of overall permeability are determined and the size of representative volume element is quantified; the concluding remarks are given in Section 5.

## 2. Bound analysis and estimate of permeability

Bound analysis is a useful tool for random heterogeneous material. In the following, three bound and estimate theories are recalled: Wiener bounds, Hashin-Shtrikman bounds and self-consistent estimate. Define concrete material as a three-phase composite: interfacial transition zone, homogeneous matrix and coarse aggregate. The material structure is arranged as such: the aggregates are coated with ITZ and distributed randomly in the matrix. The permeability and volumetric fraction of each phase are noted as $k_{ITZ}$, $k_m$, $k_{agg}$ and $f_{ITZ}$, $f_m$, $f_{agg}$ for ITZ, matrix and aggregates respectively. It is assumed that the permeability of each phase observes $k_{ITZ} > k_m > k_{agg}$. The overall permeability of composite is noted as $k_{eq}$.

### 2.1 Bound analysis

The simplest estimation of permeability for multi-phase material is the Wiener bounds, taking into account only the volumetric fraction of each phase (Wiener 1912). The Wiener bounds, $k^{+,-}_{Wiener}$, for permeability can be written as

$$\begin{cases} k^{+}_{Wiener} = \sum\limits_{i=ITZ,m,agg} k_i f_i \\ k^{-}_{Wiener} = \left( \sum\limits_{i=ITZ,m,agg} \dfrac{f_i}{k_i} \right)^{-1} \end{cases} \quad \text{with} \quad k^{+}_{Wiener} \geq k_{eq} \geq k^{-}_{Wiener} \tag{1}$$

Wiener upper bound corresponds to arrange the three phases into a laminar structure parallel to permeation direction while Wiener lower bound for permeability corresponds to a laminar structure perpendicular to permeation direction.

Hashin-Shtrikman bounds consider furthermore the isotropic distribution of different phases, thus provide bound values more realistic than Wiener bounds. Hashin-Shtrikman bounds for permeability in 2D case, $k_{HS}^{+,-}$ , observe (Hashin and Shtrikman 1962)

$$\frac{1}{2/(k_{ITZ}-k_{HS}^{+})-1/k_{ITZ}} = \sum_{i=m,agg} \frac{f_i}{2/(k_{ITZ}-k_i)-1/k_{ITZ}} \tag{2}$$

$$\frac{1}{2/(k_{HS}^{-}-k_{agg})-1/k_{agg}} = \sum_{i=ITZ,m} \frac{f_i}{2/(k_i-k_{agg})-1/k_{agg}} \tag{3}$$

### 2.2 Self-consistent estimate

Self-consistent estimate uses effective medium approximation and can better represent spherical inclusions embedded in matrix (Bruggeman 1935). To simulate the three-phase structure of concrete described as above, two "dilution" processes are taken: firstly the ITZ is incorporated into matrix to form an equivalent medium, and then aggregates are incorporated into the equivalent medium to form the final medium. According to self-consistent approximation, the permeability of equivalent medium, $k'_{eq}$, observes (Milton 2002)

$$\sum_{i=ITZ,m} f_i \frac{k_i-k'_{eq}}{k_i+2k'_{eq}} = 0 \tag{4}$$

Then the overall permeability, $k_{eq}$, can be solved by

$$(f_{ITZ}+f_m)\frac{k'_{eq}-k_{eq}}{k'_{eq}+2k_{eq}} + f_{agg}\frac{k_{agg}-k_{eq}}{k_{agg}+2k_{eq}} = 0 \tag{5}$$

### 2.3 Application

A numerical case is calculated for the above bound and estimate analysis. In this case, volumetric fractions of ITZ, matrix and aggregate are retained as 0.005, 0.595 and 0.4 respectively ($f_{ITZ}$ = 0.005, $f_m$ = 0.595, $f_{agg}$ = 0.40); the aggregates are assumed to be impermeable ($k_{agg}$ = 0). The ITZ permeability and estimated permeability are all noted in terms of the matrix permeability $k_m$. The relative permeability $k_{ITZ}/k_m$ is also noted as contrast ratio in the following context. Here the lowest permeability is $k_{agg}$ = 0, thus Wiener and Hashin-Shtrikman lower bounds are set to zero according to Eqs. (1) and (3), and the Wiener upper bound, Hashin-Shtrikman (HS) upper bound and self-consistent (SC) estimate are illustrated in terms of the local permeability of ITZ in Fig. 1.

It can be noted that the local ITZ permeability has important impact on Wiener and Hashin-Shtrikman bound values while the self-consistent estimate just varies slightly with ITZ permeability. This observation is surely related to specific phase distribution assumptions of different estimation approaches and just reflects partially the influence of ITZ on material overall permeability. The real influence of ITZ is to be quantified numerically in next section and these estimated values are to be discussed again with simulation results.

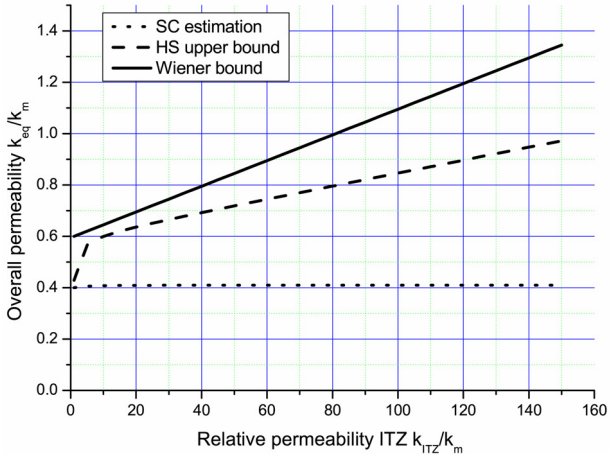


Fig. 1 Bound analysis and self-consistent estimate of overall permeability

## 3. Numerical analysis of permeability

### *3.1 Two-dimensional random aggregate structure model*

In this section numerical samples for permeability analysis are firstly established. The geometrical model is the same as aforementioned: the aggregates are coated with ITZ of specified width and together as inclusions in a homogeneous 2D matrix. The key to generate such a numerical sample is to realize the random aggregate structure (RAS) in a well-designed statistical way.

Here the generation scheme proposed by Wang *et al.* (1999), i.e. take-and-place method, is adopted. The main procedure of this scheme is described as follows: the coarse aggregates are modeled as angular polygon particles with certain elongation ratio; the sieving curve of aggregate size is divided into sieving classes and the number of particles in each class is calculated; the

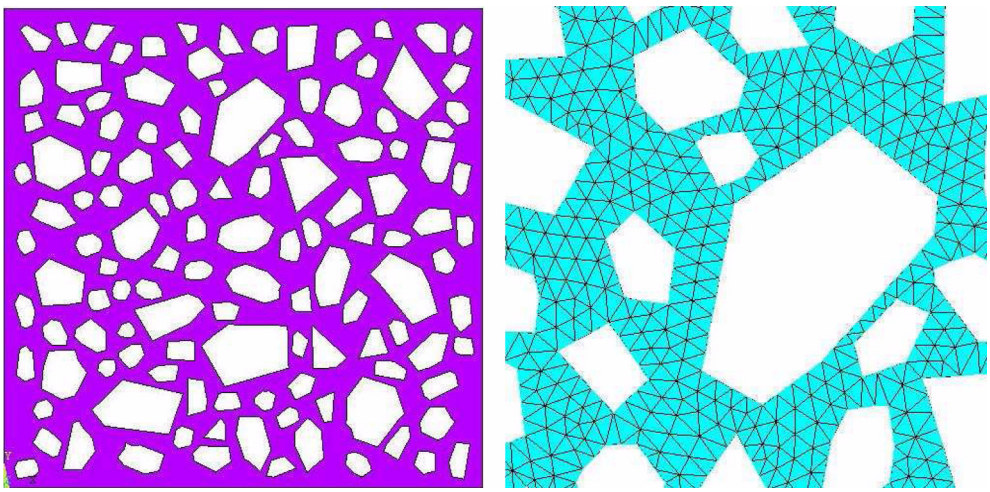

Fig. 2 Random aggregate structure (left) and matrix meshing (right)

particles packing is proceeded from large size to small size into the matrix and a minimum thickness of matrix is ensured for any two neighbored particles. A typical generated RAS sample is shown in Fig. 2 with 150 mm as square length (sample size).

In the generation of 2D random aggregate structure, the Fuller parabola is used to describe the grading distribution curve of coarse aggregate size

$$Y = 100\left(\frac{D - D_{min}}{D_{max} - D_{min}}\right)^{0.5} \tag{6}$$

where $Y$ denotes the percentage by weight passing a sieve with aperture diameter $D$, and $D_{max,min}$ denote diameters of the largest and smallest particles respectively. For numerical samples in this analysis, the elongation ratio of coarse aggregate is defined as 1.5 and $D_{min} = 5$ mm, $D_{max} = 20$ mm.

### *3.2 Finite element analysis of permeability*

Permeation is here defined as a flow process of a fluid through a porous material under a pressure gradient. For numerical analysis the fluid is assumed to observe Darcy's law, i.e. the flux $\boldsymbol{q}$ is proportional to pressure gradient $\nabla p$

$$\boldsymbol{q} = -\frac{k}{\eta}\nabla p \tag{7}$$

where $k$ is the permeability and $\eta$ the dynamic viscosity of fluid. For steady state flow, the mass conservation of fluid writes

$$\nabla \cdot \rho \boldsymbol{q} = 0 \tag{8}$$

Furthermore, if the fluid is assumed to be incompressible, like water, the fluid density $\rho$ is independent on pressure condition. In 2D cases, put Eq. (7) into Eq. (8), one gets

$$\frac{\rho k}{\eta}\left(\frac{\partial^2 p}{\partial x^2} + \frac{\partial^2 p}{\partial y^2}\right) = \frac{\rho k}{\eta}(\nabla \cdot \nabla p) = 0 \tag{9}$$

The boundary conditions, including pressure and flux conditions, are selected for a one-dimensional permeation. For the square numerical sample in Fig. 2, the pressure is imposed on two opposite sides $\Gamma_1$, $\Gamma_2$,

$$p|_{\Gamma_1} = p_1, \quad p|_{\Gamma_2} = p_2 \tag{10}$$

on the other two opposite sides is imposed a null flux condition

$$\boldsymbol{q} \cdot \boldsymbol{n}|_{\Gamma_3, \Gamma_4} = \frac{k}{\eta}\frac{\partial p}{\partial n}\bigg|_{\Gamma_3, \Gamma_4} = 0 \tag{11}$$

The Eqs. (9), (10) and (11) constitute the closed form of permeation problem. Classical finite element method is employed to solve the equations on numerical samples with fluid pressure as basic variable. Suppose the pressure gradient is imposed on the sample following $x$ direction.

Once the pressure field $p(x, y)$ is available the total flux $Q_x$ across sample can be evaluated by

$$Q_x = \int_{\Gamma_y} -\frac{k}{\eta}\frac{\partial p}{\partial x} dy \tag{12}$$

with $\Gamma_y$ as any line across numerical sample and perpendicular to flow direction. Then the overall permeability of the numerical sample can be evaluated by

$$k_{eq} = \frac{Q_x \eta}{(p_2 - p_1)} \tag{13}$$

In finite element meshing, the matrix (mortar) is discretized with 6-node triangle elements while ITZ is discretized with 2-node line elements adapted to the angular particle surface geometry. These 2-node line elements share the same nodes with particle boundaries and adopt the ITZ width $d_{ITZ}$ and ITZ permeability $k_{ITZ}$ as element properties.

### 3.3 Numerical analysis

From the literature, different observations are reported on ITZ width $d_{ITZ}$: 15~20 $\mu$m by mercury intrusion porosimetry (Snyder *et al*. 1992), 1~100 $\mu$m by backscattered electron imaging (Scrivener 2004), 30~100 $\mu$m by Wood's metal intrusion (Nemati *et al*. 1998, Nemati and Gardoni 2005). Bentz and Garboczi (1991) used ITZ width of 10~12 $\mu$m in their percolation microstructure model. Some results on local transport properties of ITZ are also available: ITZ migration coefficient of chloride ion is suggested to be 1.55, 1.76, 2.83 times of matrix migration coefficient for $d_{ITZ}$ = 20, 40, 50 $\mu$m respectively (Yang and Su 2002); effective chloride diffusion coefficient of ITZ is estimated to be 6~12 times greater than that of bulk cement paste (Bourdette *et al*. 1995).

Case study is performed on the numerical sample illustrated in Fig. 2. The aggregate volumetric fraction is retained to 0.4 and the sieving curve adopts Fuller parabola in Eq. (6). Taking into account the above literature data, the ITZ width range is retained as $d_{ITZ}$ = 0~100 $\mu$m, and three contrast ratios are retained for ITZ permeability: $k_{ITZ}/k_m$ = 10, 50, 100. In this analysis the possible change of ITZ width with aggregate size is neglected. The overall permeability is solved through the numerical scheme established in last section, and the relative overall permeability, $k_{eq}/k_m$, is illustrated in function of ITZ width dITZ, cf. Fig. 3.

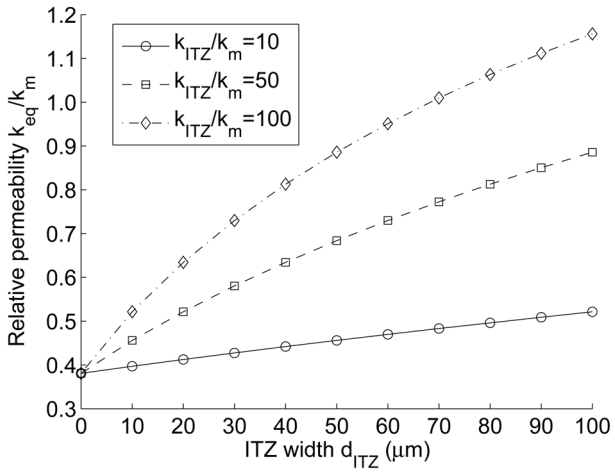


Fig. 3 Impact of ITZ on overall permeability for different contrast ratios

### 3.4 Influence of aggregates and ITZ

As indicated by available research (Delagrave *et al.* 1997, Garboczi *et al.* 1995, Schwartz *et al.* 1995), incorporating impermeable aggregates in a homogeneous matrix globally has two opposite effects: the dilution and tortuosity effects of aggregates reduces material overall permeability while ITZ with high local permeability increases it.

The first observation of Fig. 3 is the important hindering effect of randomly distributed aggregates on permeation process. According to the straightforward estimation ofWiener bound in Eq. (1), the relative overall permeability $k_{eq}/k_m$ will be 0.6 for $f_{agg}$ = 0.4 and $d_{ITZ}$ = 0. Theoretically this can be regarded as the pure dilution effect of the inclusion of impermeable aggregates. However, Fig. 3 shows that $k_{eq}/k_m$ is further decreased to 0.38. The impermeable aggregates force the fluid to flow around them thus create a "tortuosity" effect. The adopted aggregate volume fraction is rather representative for conventional concrete in practice. Thus the dilution and tortuosity effects of randomly distributed aggregates are the first two important factors to be considered in permeability estimation.

Then, the ITZ influence on overall permeability depends on its width and local permeability, and the contrast ratio $k_{ITZ}/k_m$ plays an important role. For low contrast ratio $k_{ITZ}/k_m$ = 10, the overall permeability increases almost linearly with ITZ width (volumetric fraction), i.e. the increase of overall permeability is proportional to ITZ width or volumetric fraction. But the increase range is rather limited: $k_{eq}/k_m$ = 0.38~0.52 for $d_{ITZ}$ = 0~100 $\mu$m. For larger contrast ratios $k_{ITZ}/k_m$ = 50, 100, the overall permeability increases nonlinearly with the ITZ width with more important increase ranges. For $k_{ITZ}/k_m$ = 50, the relative overall permeability attains 0.6 as $d_{ITZ}$~35 $\mu$m, i.e. the ITZ compensates completely the tortuosity effect of impermeable aggregates. For $k_{ITZ}/k_m$ = 100, $d_{ITZ}$ = 70 $\mu$m, the relative overall permeability overpasses 1.0, meaning the ITZ "cancels" both dilution and tortuosity effects of aggregates in matrix. It is to be noted that the nonlinear relationship $k_{eq}/k_m$-$d_{ITZ}$ is not due to ITZ percolation but the pure effect of ITZ volumetric fraction increase.

In the above analysis the ITZ volumetric fraction can be deduced from ITZ width. The volumetric fraction $f_{ITZ}$ = 0.005, retained in the bound/estimate analysis in Section 2, corresponds to $d_{ITZ}$ = 30 $\mu$m. In Table 1 are compared the numerical simulation results and estimation values of overall permeability. For $\lambda$ = 1, the ITZ is merged completely into the matrix thus the overall permeability can be read in Fig. 3 for $d_{ITZ}$ = 0. From the table, it can be seen that: (1) Wiener and Hashin-Shtrikman bounds can well envelop the simulation values but with a rather large margin; (2) self consistent estimates approach the simulation values for low contrast ratios, $\lambda$ = 1, 10, but underestimate the permeability for high contrast ratios, $\lambda$ = 50, 100.

Table 1. Comparison of simulation and estimation values of overall permeability

| Method | $\lambda$ = 1 | $\lambda$ = 10 | $\lambda$ = 50 | $\lambda$ = 100 |
|---|---|---|---|---|
| Wiener bound (upper) | 0.600 | 0.645 | 0.845 | 1.095 |
| Hashin-Shtrikman bound (upper) | 0.429 | 0.599 | 0.718 | 0.846 |
| Self-consistent estimate | 0.400 | 0.407 | 0.409 | 0.410 |
| Numerical simulation | 0.381 | 0.412 | 0.521 | 0.634 |

## 4. Statistical analysis of permeability

Numerical samples of different sizes are generated randomly in this section and the statistical characteristics of overall permeability are analyzed. Then a concept closely related to the statistical characteristics of overall permeability, representative volume element (RVE), is discussed in terms of numerical sample size and expected simulation error.

### *4.1 Permeability analysis of random samples*

Numerical sample sizes are scaled from 80 mm to 300 mm with 10 mm as increase grade. For each sample size 40 random aggregate structures are generated with $D_{min,max}$ = 5, 20 mm, $f_{agg}$ = 0.40 and distribution obeying Fuller's curve in Eq. (6). The ITZ width is retained as $d_{ITZ}$ = 30 $\mu$m and four permeability contrast ratios are taken: $\lambda = k_{ITZ}/k_m$ = 1, 10, 50, 100. Thus, totally 3680 simulations are performed for overall permeability analysis with 920 simulations for each contrast ratio. The numerical simulation results and the mean values are presented in Fig. 4.

From the figure, two important observations can be made. Firstly, the dispersion of overall permeability decreases substantially with the increase of sample size, relative error ranging from ~8% for 80 mm and ~2% for 300 mm. This size-dependent dispersion is characteristic for properties of random

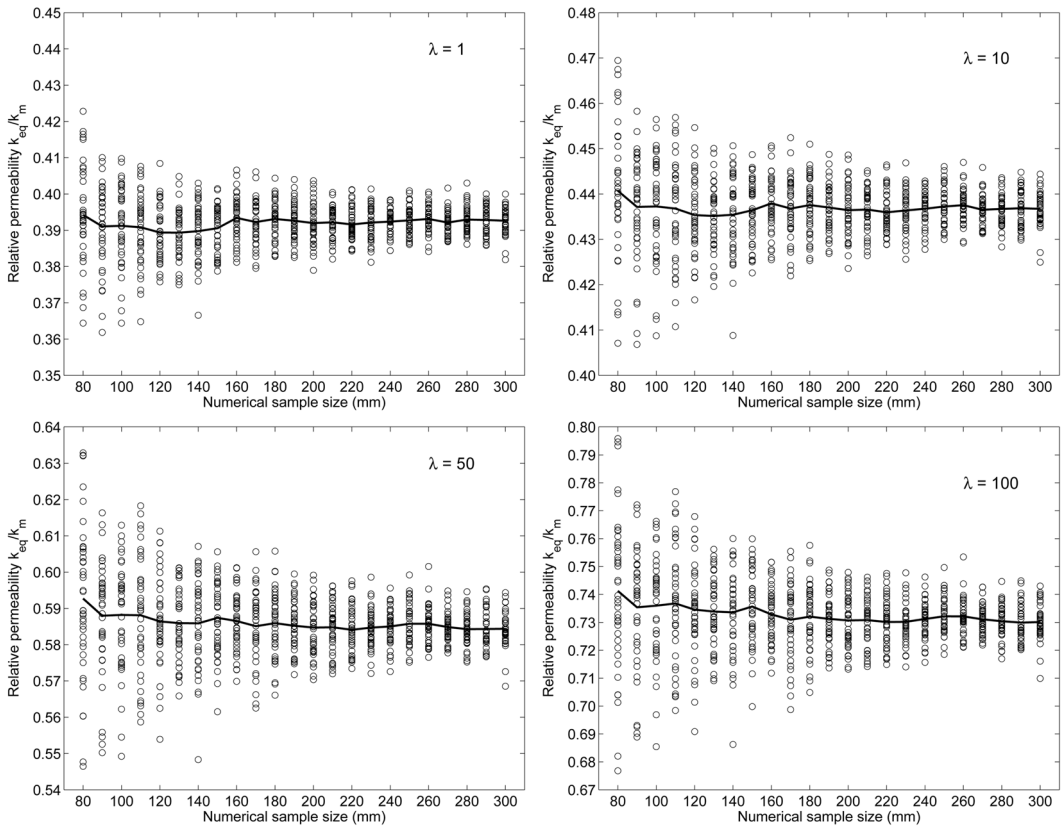


Fig. 4 Overall permeability and its dispersion for different contrast ratios (solid lines for mean values)

heterogeneous composites. Theoretically this dispersion can disappear as the sample attains the size of representative volume element (RVE). Secondly, the contrast ratio influences both the permeability mean values and the dispersion extent: higher contrast ratios give larger overall permeability as well as larger absolute dispersion. These two aspects are to be quantified and analyzed further in next section.

### *4.2 Variance analysis of permeability*

To explore the statistical characteristics of overall permeability in terms of sample size and ITZ properties, the overall permeability is considered to be an ergodic stationary random function (Lantuéjoul 1991). Then a power law of scaling property (Kanit *et al.* 2003, Pelissou *et al.* 2009) is retained for the variance of overall permeability

$$D_k^2(A) = D_k^2 \times \left(\frac{A_2}{A}\right)^{\alpha} \tag{14}$$

In this equation, $A$ stands for the numerical sample size; $A_2$ denotes the integral range of the three-phase composite, scaling the domain size for stabilized variance of the random function (Lantuéjoul 1991); $D_k$ represents the point variance of local permeability of different phases in random composite and $D_k^2(A)$ represents the permeability variance of realized numerical samples of size $A$. It should be noted that the relation in Eq. (14) is just one of the available scaling laws and the spatial correlation between different phases is fundamental for this scaling law. The above relation can be converted to linear relationship in logarithm scale

$$\log[D_k^2(A)] = -\alpha\log(A) + [\log(D_k^2) + \alpha\log(A_2)] \tag{15}$$

In our case, the point variance of permeability can be calculated by

$$D_k^2 = \sum_{i=ITZ,m,agg} k_i^2 f_i - \left(\sum_{i=ITZ,m,agg} k_i f_i\right)^2 \tag{16}$$

Using Eq. (15) and $D_k^2$ values, the variance of overall permeability in Fig. 4 is fitted for different contrast ratios. The relevant fitting results are presented in Table 2 and Fig. 5. The correlation coefficient $R > 0.999$ indicates that the power law is well-suited. The integral range $A_2$ decreases sharply as contrast ratio increases because of the small fraction but high local permeability of ITZ, cf. Eq. (16). The scaling exponent $\alpha$ is close to 1, meaning the variance decreases almost inversely with sample size increase.

Furthermore, one can see that higher contrast ratio has larger scaling exponent: $\alpha = 1.037$ for $\lambda = 1$ and $\alpha = 1.172$ for $\lambda = 100$. In other words, the variance of overall permeability decreases

Table 2. Fitting parameters for variance analysis of overall permeability

| Contrast ratio $\lambda$ (–) | Point variance $D_k^2$ (–) | Integral range $A_2$ (mm$^2$) | Scaling exponent $\alpha$ (–) |
|---|---|---|---|
| 1 | 0.240 | 5.684 | 1.037 |
| 10 | 0.679 | 3.947 | 1.097 |
| 50 | 12.38 | 0.931 | 1.166 |
| 100 | 49.40 | 0.476 | 1.172 |

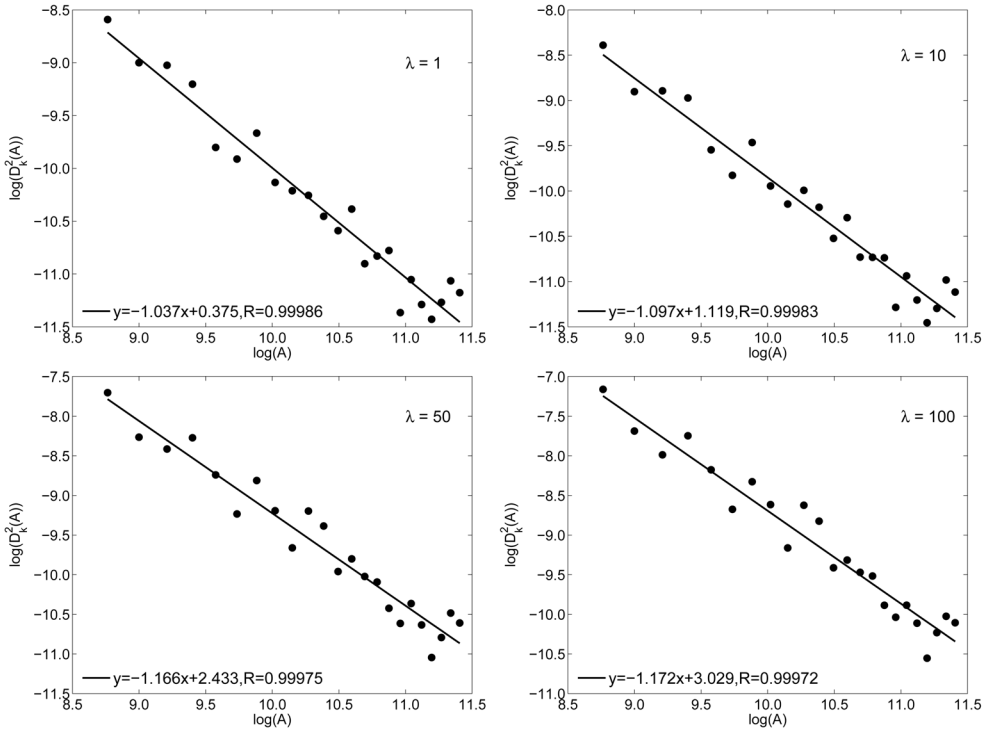


Fig. 5 Power law fitting of permeability variance for different contrast ratios

more rapidly with sample size for higher contrast ratios. Thus the ITZ of higher local permeability helps to stabilize the fluctuation of overall permeability. This observation is due to the specific structure of three-phase composite retained for concrete: impermeable aggregates coated by ITZ and dispersed in matrix. During the permeation process, an ITZ layer with higher local permeability, $k_{ITZ} > k_m$, renders the coated aggregates "permeable" to some extent. Considering $f_{ITZ}$ is very small, higher $k_{ITZ}$ will render the permeability of coated aggregates closer to that of matrix. This effect decreases actually the contrast of permeability between matrix and the coated aggregates, so the composite is more homogeneous during permeation. That explains why higher $\lambda = k_{ITZ}/k_m$ helps to converge the overall permeability.

### 4.3 RVE size estimation

In homogenizing the random heterogeneous composites, the concept of representative volume element (RVE) is involved. Hashin (1983) defined RVE as: "The RVE is a model of the material to be used to determine the corresponding effective properties for the homogenized macroscopic model. The RVE should be large enough to contain sufficient information about the microstructure in order to be representative, however it should be much smaller than the macroscopic body". Thus RVE is both microstructure-dependent and property-dependent. For a same composite, different physical processes can have different RVE definition (Drugan and Willis 1996, Graham and Yang 2002, Gitman *et al.* 2007). In this section, the RVE for permeability is investigated.

Theoretically, if the sample size attains RVE size the overall permeability dispersion will vanish.

Numerically this dispersion will decrease as the sample size increases, cf. Fig. 4, but will never vanish. Thus, the numerical determination of RVE size is always associated with an expected error. According to sample theory, the relative error $\varepsilon_r$ with respect to mean value $M$ obtained with $N$ independent realizations for a given sample size $A$ is written as

$$\varepsilon_r = \frac{2D_k(A)}{M\sqrt{N}} \tag{17}$$

Taking into account Eq. (14), the sample size with respect to a given $\varepsilon_r$ is

$$A = A_2\left(\frac{4D_k^2}{\varepsilon_r^2 M^2 N}\right)^{1/\alpha} \tag{18}$$

As the realization number $N = 1$, the sample size at the left side of equation becomes RVE size. With the fitting parameters in Table 2, the RVE size is determined for all contrast ratios at three error levels: 1%, 2% and 5%, cf. Table 3. Moreover, the standard deviation $D_k(A)$ and the variation coefficient $D_k(A)/M$ in Eq. (17) are illustrated in Fig. 6 in terms of sample sizes.

From Table 3, one can see that both contrast ratio and expected error have important impact on RVE size, i.e. 21.1~24.5$D_{max}$ for $\varepsilon_r = 1\%$ and 5.1~5.5$D_{max}$ for $\varepsilon_r = 5\%$. For a same contrast ratio $\lambda$, the RVE size decreases rapidly as the error increases. For a given error level, the influence of ITZ permeability on RVE size is less important but not straightforward. In fact, higher contrast ratios lead to larger permeability mean value, cf. Fig. 4; the standard deviation of permeability for higher contrast ratios is larger but decreases more rapidly, cf. Fig. 6. The variation coefficient in Fig. 6

Table 3. RVE size estimation for three error levels $\varepsilon_r = 1\%$, 2% and 5%

| Contrast ratio $\lambda$ (–) | RVE size (mm) | | | RVE size/$D_{max}$ (–) | | |
|---|---|---|---|---|---|---|
| | $\varepsilon_r$ =1% | $\varepsilon_r$ =2% | $\varepsilon_r$ =5% | $\varepsilon_r$ =1% | $\varepsilon_r$ =2% | $\varepsilon_r$ =5 |
| 1 | 489.3 | 250.8 | 103.7 | 24.5 | 12.5 | 5.2 |
| 10 | 443.6 | 235.8 | 102.3 | 22.2 | 11.8 | 5.1 |
| 50 | 422.8 | 233.3 | 106.3 | 21.1 | 11.7 | 5.3 |
| 100 | 435.9 | 241.3 | 110.4 | 21.8 | 12.1 | 5.5 |

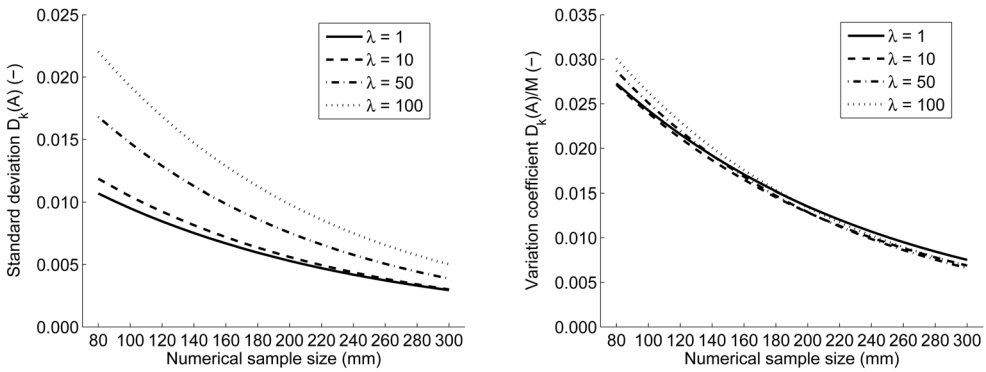


Fig. 6 Standard deviation (left) and variation coefficient (right) in terms of sample sizes

Table 4. Required sample size in terms of available realization number for $\varepsilon_r = 1\%$

| Contrast ratio $\lambda$ (−) | Required sample size (mm) | | | Required sample size/$D_{max}$ (−) | | |
|---|---|---|---|---|---|---|
| | N=1 | N=3 | N=5 | N=1 | N=3 | N=5 |
| 1 | 489.3 | 288.1 | 225.2 | 24.5 | 14.4 | 11.3 |
| 10 | 443.6 | 268.8 | 213.0 | 22.2 | 13.4 | 10.7 |
| 50 | 422.8 | 263.9 | 212.0 | 21.1 | 13.2 | 10.6 |
| 100 | 435.9 | 272.8 | 219.4 | 21.8 | 13.6 | 11.0 |

takes into account all these factors. The synthetic result is: lower contrast ratio tends to have larger RVE size at low error level but smaller RVE size at high error level.

Another important application of Eq. (18) is to establish the relationship between the sample size and realization number for an expected error level. In Table 4 are presented the required sample size and available realization number for a given error of 1%. From Table 4, one can see that augmenting sample number is efficient to reduce the required sample size, i.e. 21.1~24.5$D_{max}$ for N=1 and 10.6~11.3$D_{max}$ for N=5.

## 5. Conclusions

1. In this paper three-phase composite model is adopted to describe the permeability of concrete materials. The coarse aggregates are coated with ITZ and dispersed randomly in a homogeneous matrix. Firstly, different bound and estimate values are calculated for this model. From the case analysis, Wiener bound and Hashin-Shtrikman bound values are substantially influenced by ITZ local permeability while the self-consistent estimate just changes slightly in terms of ITZ local permeability. The later is related to the very tiny volumetric fraction of ITZ, i.e. $f_{ITZ} = 0.005$. The comparison between estimation and numerical simulation results shows that Wiener and Hashin-Shtrikman upper bounds envelop well the overall permeability but with a rather large margin while self-consistent estimates can best approach the numerical results at low contrast ratio, $k_{ITZ}/k_m$.

2. Two dimensional random aggregate structure (RAS) is employed to generate numerical sample of three-phase composite model. The aggregates are modeled as angular particles with a certain elongation ratio and Fuller's parabola is attributed to the size distribution of particles. The steady flow of fluid permeation process in material is described by Laplace's equation with constant pressure gradient boundary condition and the pressure field in numerical sample is solved by classical finite element method. Numerical analysis on the overall permeability shows that as the contrast ratio, $k_{ITZ}/k_m$, is moderate, overall permeability increases proportionally with ITZ volumetric fraction while nonlinearity arises as the contrast ratio becomes important. In extreme cases, the contribution of ITZ to overall permeability can cancel completely the tortuosity effect and dilution effect of impermeable aggregates.

3. Totally 3680 numerical samples are generated to investigate the statistical characteristics of overall permeability. Power scaling law is well adapted to the overall permeability variance. As the volumetric fractions of ITZ and aggregate hold constant, larger contrast ratio gives more important permeability dispersion and helps to stabilize the fluctuation of overall permeability. The later is explained by the specific three-phase composite structure, i.e. impermeable aggregates coated with

ITZ and dispersed in matrix. The ITZ layer with larger local permeability renders the coated aggregates "permeable", which, in fact, decreases the contrast of local permeabilities between the matrix and coated aggregates.

4. The RVE size of such a composite model is established through sample theory, giving explicit relationship among the required sample size, expected relative error and available realization number. For realization number equal to 1, the RVE sizes are calculated for given errors and expressed in terms of maximum particle size. The results show that error level has more important impact on RVE size and the influence of ITZ on RVE size is not straightforward. Furthermore, the relation of required sample size versus realization number is also calculated, this relation can be particularly useful for numerical simulation and experiment planning. For numerical simulation, as the sample size is held constant, required sample number can be calculated for a given error level; for experimental planning, as the sample (specimen) number is limited, the minimum specimen size can be estimated for an expected precision.

## Acknowledgements

This work was supported by a grant from the Major State Basic Research Development Program of China (973 Program) (No.2009CB623106).

## References

AFGC (French Association of Civil Engineering) (2007), *Concrete design for a given structure service life, State-of-the-art and guide for the implementation of a predictive performance approach based upon durability indicators*, AFGC Scientific and Technical Documents, Paris.

Bentz, D.P. and Garboczi, E.J. (1991), "Percolation of phases in a three-dimensional cement paste microstructural model", *Cement Concrete Res.*, **21**(2), 325-344.

Bourdette, B., Ringot, E. and Ollivier, J.P. (1995), "Modelling of the transition zone porosity", *Cement Concrete Res.*, 25(4), 741-751.

Bruggeman, D.A.G. (1935), "Calculation of various constants in heterogeneous substances. I. Dielectric constants and conductivity of composites from isotropic substances", *Ann. Phys.*, **24**, 636-679. (in German)

Delagrave, A., Bigas, J.P., Ollivier, J.P., Marchand, J. and Pigeon, M. (1997), "Influence of the interfacial zone on the chloride diffusivity of mortars", *Adv. Cement Base. Mater.*, **5**(3), 86-92.

Drugan, W.J. and Willis, J.R. (1996), "A micromechanics-based nonlocal constitutive equation and estimates of representative volume element size for elastic composites", *J. Mech. Phys. Solids*, **44**(4), 497-524.

El-Dieb, A.S. and Hooton, R.D. (1995), "Water permeability measurement of high performance concrete using high-pressure triaxial cell", *Cement Concrete Res.*, **25**(6), 1199-1208.

Garboczi, E.J., Schwartz, L.M. and Bentz, D.P. (1995), "Modeling the influence of the interfacial zone on the DC electrical conductivity of mortar", *Adv. Cement Base. Mater.*, **2**(5),169-181.

Gitman, I.M., Askes, H. and Sluys, L.J. (2007), "Representative volume: existence and size determination", *Eng. Fract. Mech.*, **74**(16), 2518-2534.

Graham, S. and Yang, N. (2002), "Representative volumes of materials based on microstructural statistics", *Scripta Mater.*, **48**(3), 269-274.

Hashin, Z. and Shtrikman S. (1962), "A variational approach to the theory of the effective magnetic permeability of multiphase materials", *J. Appl. Phys.*, **33**, 3125-3131.

Hashin, Z. (1983), "Analysis of composite materials-a survey", *J. Appl. Mech.*, **50**, 481-505.

Hu, J. and Stroeven P. (2004), "Properties of the interfacial transition zone in model concrete", *Interface Sci.*,

**12**(4), 389-397.
Kanit, T., Forest, S., Galliet, I., Mounoury, V. and Jeulin, D. (2003), "Determination of the size of the representative volume element for random composites: statistical and numerical approach", *Int. J. Solids Struct.*, **40**(13), 3647-3679.
Kollek, J.J. (1989), "The determination of the permeability of concrete to oxygen by the Cembureau method - a recommendation", *Mater. Struct.*, **22**, 225-230.
Lantuéjoul, C. (1991), "Ergodicity and integral range", *J. Microscopy*, **161**, 387-403.
Maekawa. K., Ishida, T. and Kishi, T. (2009), *Multi-scale modeling of structural concrete*, Taylor & Francis, London and New York.
Milton, G.W. (2002), *The theory of composites*, Cambridge University Press, Cambridge, UK.
Nemati, K.M., Monteiro, P.J.M. and Scrivener, K.L. (1998), "Analysis of compressive stress-induced cracks in concrete", *ACI Mater. J.*, **95**(5), 617-630.
Nemati, K.M. and Gardoni, P. (2005), "Microstructural and statistical evaluation of interfacial zone percolation in concrete", *Strength, Fracture Complexity*, **3**(2), 191-197.
Ollivier, J.P., Maso, J.C. and Bourdette, B. (1995), "Interfacial transition zone in concrete", *Adv. Cement Base. Mater.*, **2**(1), 30-38.
Pelissou, C., Baccou, J., Monerie, Y. and Perales, F. (2009), "Determination of the size of the representative volume element for random quasi-brittle composites", *Int. J. Solids Struct.*, **46**(14), 2842-2855.
Powers, T.C. (1958), "Structure and physical properties of hardened portland cement paste", *J. Am. Ceram. Soc.*, **41**(1), 1-6.
Reinhardt, H.W.(ed.) (1997), *Penetration and permeability of concrete: barriers to organic and contaminating liquids*, RILEM Report 16, E&FN Spon, London.
Schwartz, L.M., Garboczi, E.J. and Bentz, D.P. (1995), "Interfacial transport in porous media: application to dc electrical conductivity of mortars", *J. Appl. Phys.*, **78**(10), 5898-5908.
Scrivener, K.L. and Gartner, E.M. (1988), "Microstructural gradient in cement paste around aggregate particles", *Mater. Res. Soc. Symp. Proc.*, **114**, 77-85.
Scrivener, K.L. (2004), "Backscattered electron imaging of cementitious microstructures: understanding and quantification", *Cement Concrete Comp.*, **26**(8), 935-945.
Snyder, K.A., Winslow, D.N., Bentz, D.P. and Garboczi, E.J. (1992), "Effects of interfacial zone percolation on cement based composite transport properties", *Materials Research Society Symposium Proceedings*, *Advanced Cement Based Systems: Mechanisms and Properties,* **245**, 265-270.
van Mier, J.G.M. (1997), *Fracture processes of concrete*, CRC Press, US.
Wang, Z.M., Kwan, A.K.H. and Chan, H.C. (1999), "Mesoscopic study of concrete I: Generation of random aggregate structure and finite element mesh", *Comput. Struct.*, **70**(5), 533-544.
Wiener, O. (1912), "The theory of composites for the field of steady flow. First treatment of mean value estimates for force, polarization and energy", *Abhandlungen der mathematischphysischen Klasse der Koniglich Gesellschaft der Wissenschaften*, **32**, 509-604. (in German)
Yang, C.C. and Su, J.K. (2002), "Approximate migration coefficient of interfacial transition zone and the effect of aggregate content on the migration coefficient of mortar", *Cement Concrete Res.*, **32**(10), 1559-1565.

*CM*